Effect of mixing ratios of SiO$_2$ nanoparticles synthesized from metakaolin on the physicochemical properties of ZnO/SiO$_2$ nanocomposites

Elijah Yanda Shaba *, Jimoh Oladejo Tijani, John Olusanya Jacob, Mohammed Abubakar Tanko Suleiman

Department of Chemistry, Federal University of Technology, P. M. B. 65, Minna, Niger State, Nigeria
Nanotechnology Research Group, African Centre of Excellence of Mycotoxins and Food Safety (ACEMFS), Federal University of Technology, P. M. B. 65, Bosso Campus, Minna, Niger State, Nigeria

ARTICLE INFO

ABSTRACT

Nanomaterials have distinguished themselves as an outstanding class of materials due to their unique physical and chemical characteristics compared to bulk materials. The physicochemical properties of nanomaterials can be improved by forming nanocomposites and manipulating different nanoparticles by varying their mixing ratios. In this study, ZnO and SiO$_2$ nanoparticles and ZnO/SiO$_2$ nanocomposites were produced using a sol–gel method based on the variation of mixing ratios (1:1, 1:2 and 2:1). The monometallic oxide nanoparticles (ZnO, SiO$_2$) and the corresponding nanocomposites (ZnO/SiO$_2$) were characterized using HRSEM, EDX, XRD, FTIR, BET and XPS. Regardless of the mixing ratio of ZnO and SiO$_2$ nanoparticles used, the HRSEM pictures demonstrated a morphological change from the irregular and spherical forms produced for SiO$_2$ and ZnO nanoparticles to rod-like shapes for the ZnO/SiO$_2$ nanocomposite. The quartz phase of SiO$_2$ nanoparticles, with a crystallite size of 43.67 nm, and the hexagonal wurtzite phase of ZnO nanoparticles, with a crystallite size of 31.52 nm, were both synthesized, as revealed by the XRD results. As opposed to this, the XRD patterns of the ZnO/SiO$_2$ nanocomposites synthesized with 1:1, 1:2 and 2:1 mixing ratios showed a mixture of α-quartz (SiO$_2$) and hexagonal wurtzite (ZnO) with crystallite sizes of 21.24, 29.56 and 15.36 nm, respectively. The EDS results confirmed the existence of Zn and O for ZnO; Si and O for SiO$_2$ nanoparticles and Zn, Si and O in the prepared ZnO/SiO$_2$ nanocomposite, irrespective of the mixing ratios. The XPS results showed the existence of Zn in the +1 oxidation state in ZnO/SiO$_2$ compared to single ZnO with the Zn^{2+} valence. The BET surface area indicates that the ZnO/SiO$_2$ nanocomposites had a higher surface area (1:1 (39.042 m^2/g), 1:2 (55.602 m^2/g) and 2:1 (82.243 m^2/g)), irrespective of the mixing ratios, compared to the surface area for the ZnO (8.620 m^2/g) and SiO$_2$(0.386 m^2/g) nanoparticles. The mixing ratio of the ZnO and SiO$_2$ nanoparticles influenced the crystallite sizes, surface elements oxidation states and morphology of the ZnO/SiO$_2$ nanocomposite formed and the optima mixing ratio for the formation of ZnO/SiO$_2$ nanocomposite was found to be 2:1 of ZnO:SiO$_2$ nanoparticles.

1. Introduction

Nanotechnology has gained considerable attention among researchers as one of the innovative technologies of the 21st century that has transformed numerous sectors of the economy across the globe [1]. Nanomaterials differ from their macroscale counterparts in several ways, such as high surface-to-volume ratio, compatibility with other materials and high porosity [2]. All these properties have made scientists search for nanomaterials that could be used for diverse applications. For instance, ZnO nanoparticles have been synthesized for application in wastewater treatment, medicine, electronics, paints and food industries [3–5]. ZnO nanoparticles are a promising material due to their distinctive characteristics, which include excellent chemical and thermal stability, low cost, non-toxicity, excellent cycling stability, simplicity in production and compatibility with other materials [6,7]. ZnO is an n-type semiconductor with a wide-band gap energy of 3.37 eV [8,9]. ZnO nanoparticles are one of the most widely produced nanomaterials, they are frequently used in sunscreen, research, food packaging and analytical sensing applications [10]. ZnO nanoparticles have demonstrated several biological and therapeutic applications, such as photocatalysts, with biocompatibility, antibacterial, anticancer, antileishmanial, antioxidant and enzyme inhibitory

* Corresponding author.
  E-mail address: elijah.shaba@futminna.edu.ng (E.Y. Shaba).

effects [11]. Additionally, ZnO nanoparticles have been added to base oils as additives to enhance their lubricating qualities.

Recently, SiO$_2$ nanoparticles have drawn a lot of attention since they are simple to utilize and stable across all pH ranges (basic and acidic), have low toxicity, exceptional biocompatibility, superior mechanical qualities, the capacity to be functionalized with a variety of other metal oxides and controlled particle sizes [12,13]. However, SiO$_2$ is usually synthesized from chemical sources, such as sodium silicate and tetraethylorthosilicate, which are costly and generate secondary pollutants [14]. The synthesis of SiO$_2$ nanoparticles from other materials, including waste from agriculture products, such as corn cob, rice husk, palm trash and coconut shell, that are reportedly environmentally friendly, have been cited in the literature [15,16]. Recent studies have shown that readily available materials such as kaolin, with a high amount of silica compared to other agricultural wastes, have been utilized in the production of SiO$_2$ nanoparticles [17]. The clay mineral called kaolin contains silica (SiO$_2$) in high concentrations with high single silica, also the abundant and reasonably priced kaolin clay contains the by-product alumina. This naturally available material has been reported to serve as a precursor for the production of SiO$_2$ nanoparticles. For example, Tijani et al. [18] produced SiO$_2$ nanoparticles from dealuminated metakaolin at different pH values of 5, 8 and 10, and different NaOH concentrations (0.5, 1 and 2 M); the final product was calcined in a furnace at 600, 700 and 800 °C. The authors reported that the SiO$_2$ nanoparticles were highly crystalline. Different methods, such as solvothermal, hydrothermal, chemical vapour deposition, arc discharge and sol–gel methods, have been used for the synthesis of nanoparticles and their composites [19]. Among the aforementioned methods, the sol–gel method is recognized as a simple and easy method for the synthesis of nanomaterials.

Despite the successes recorded in the production and application of monometallic oxide nanoparticles through the years, the use of monometallic oxide nanoparticles has been associated with some drawbacks, such as *instability* [20], agglomeration [21], difficulty in *recovering after application* [22] and low efficiency compared with nanocomposites [23]. Due to the aforementioned problems associated with the application of monometallic oxide nanoparticles, the modification of the surface of monometallic nanoparticles such as ZnO with another metal oxide, like SiO$_2$ nanoparticles, to produce novel material with unique properties for diverse applications is desirable. For instance, M. Justine et al. [24] synthesized a ZnO/SiO$_2$ nanocomposite via the sol–gel method and reported that the phase of ZnO nanoparticles remains hexagonal shaped after the formation of the ZnO/SiO$_2$ nanocomposite. They found that the ZnO/SiO$_2$ nanocomposites have a smaller crystallite size (34.09 nm) than single ZnO nanoparticles (44.37 nm). The authors synthesized the SiO$_2$ nanoparticles from tetra ethyl ortho silicate (TEOS). Additionally, Fida'I et al. [25] synthesized ZnO/SiO$_2$ nanocomposites. The authors used the solid-state method to form ZnO/SiO$_2$ nanocomposites using a 1:1 mixing ratio of ZnO nanoparticles and palm waste silica. The authors subjected the ZnO/SiO$_2$ nanocomposites to calcination at different temperatures (600, 800, 1000, 1200 and 1400 ∘C). Their research findings indicated that as the calcination temperature increased, the intensity and the crystallinity of the ZnO/SiO$_2$ nanocomposites increased. Additionally, the authors reported that the nanocomposites aggregate as the temperature increased and an irregular particle shape was observed. Numerous studies have been conducted on the formation of ZnO/SiO$_2$ nanocomposites through surface modification of ZnO nanoparticles. These researchers frequently ignored the effect of the mixing ratios of both the ZnO and SiO$_2$ nanoparticles and their effect on the physicochemical properties of the ZnO/SiO$_2$ nanocomposites formed. Additionally, many researchers utilize commercially available chemicals as precursors for the production of SiO$_2$

nanoparticles, where these chemicals are toxic and have long term effects. Due to their compact size, high surface area and relationships of phases at their interfaces, ZnO/SiO$_2$ nanocomposites offer unique features. ZnO/SiO$_2$ nanocomposites have the potential to produce high-value materials, such as catalysts, medicines, biomaterials and environmental remediation.

In this research, the authors describe the synthesis of nanocomposites (ZnO/SiO$_2$) based on varying mixing ratios using SiO$_2$ nanoparticles synthesized from metal kolin for the first time. The SiO$_2$ nanoparticles were synthesized from locally available kaolin in Niger State, Nigeria. Additionally, the authors compared the physicochemical properties of the ZnO/SiO$_2$ nanocomposites synthesized with different mixing ratios of the single monometallic oxides (ZnO and SiO$_2$). The nanocomposites (ZnO/SiO$_2$) produced were characterized using high-resolution scanning electron microscopy (HRSEM) and Fourier transform infrared (FTIR), X-ray photoelectrons spectroscopy (XPS), and X-ray diffraction (XRD).

2. Experimental section

Analytical grade sodium hydroxide (93%) zinc nitrate hexahydrate (98%) and polyvinyl pyrrolidone (PVP) (95%) were provided by Sigma Aldrich and was used without further purification.

2.1. Synthesis of the zinc oxide/silicon oxide (ZnO/SiO$_2$) nanocomposites

The ZnO nanoparticles were synthesized by stirring 50 mL of 0.1 M Zn(NO$_3$)$_2$· 6H$_2$O at 250 rpm for two minutes at ambient temperature in a 250 mL beaker using a magnetic stirrer. 25 mL of 1.0 M NaOH solution was added to the solution, followed by the addition of 10 mL 5% polyvinylpyrrolidone to the same solution. This formed a sol–gel-like solution, which was dried at 100 °C before being calcined at 450 °C for 2 h.

Furthermore, SiO$_2$ was synthesized by measuring 5 g of de-aluminium metakaolin into a 250 mL beaker, then 60 mL of water were added. The solution was stirred for 15 min, then 30 mL of 0.3 M NaOH was added and the mixture was stirred continuously at ambient temperature for 30 min. The obtained mixture was allowed to stand for 24 h and then dried at 100 °C in an oven for 24 h. Next, it was calcined at 450 °C for 2 h to give SiO$_2$ nanoparticles. Finally, to synthesize the ZnO/SiO$_2$ nanocomposites, 50 mL distilled water was measured into a 250 mL beaker and 5 g of Zn(NO$_3$)$_2$· 6H$_2$O and 5 g of de-aluminium metal kaolin, to give a 1:1 mixing ratio, were added. The beaker was sealed with aluminium foil sheets and stirred for 10 min with a magnetic stirrer. Next 30 mL of 0.3 M NaOH and 10 mL of polyvinylpyrrolidone (5%) were added to the same solution and stirred for 30 min at ambient temperature. The solution was allowed to stand overnight. This procedure was repeated for the synthesis of ZnO/SiO$_2$ nanocomposites with mixing ratios of 1:2 and 2:1. In each case, the nanocomposites (ZnO/SiO$_2$) synthesized were dried for an hour at 100 °C in an oven and later calcined at 450 °C in a furnace for 2 h.

2.2. Characterization of ZnO, SiO$_2$ and ZnO/SiO$_2$ nanocomposites

To determine the phases and the crystal structures of the produced nanoparticles and nanocomposites, CuK$_\alpha$ radiation with a wavelength of 1.5406 Å was used with an X-ray diffraction (XRD) Bruker D8 diffractometer. A degreased glass slide was used to disseminate the powdered materials, and a scanned and scattering signal was generated from 20 to 70°. The data were compared to the diffraction pattern from the Joint Committee on the Powder Diffraction Standard and the existing d-spacing data

(JCPDS). The surface morphology of the produced nanocomposites was examined using HRSEM (Zeiss Auriga HRSEM). Au/Pd was applied to each prepared sample (0.05 mg), which was then put on carbon tape. The microscope was operated with a 5 kV high electron tension for imaging.

The functional groups of the prepared samples were examined using an FTI-R Thermo Scientific Nicolet iS5 instrument to identify different bond stretching bands. The measurements were performed in the wavenumber range of 4000–500 cm^{-1}. For these studies, a 0.2 V AC voltage was supplied to the sample. Data collection and result fitting were performed using WINDETA and ZView software. X-ray photoelectron spectroscopy (XPS) (PHI5000 versa probe UL VAC instrument) was employed to examine and analyse the oxidation state of each sample. The BET N_2 adsorption–desorption method was used to determine the surface area of the nanoscale materials. Using a nitrogen adsorption–desorption study at 76.5 K, the BET Nova 1200e (Quantachrome) physisorption analyzer was employed in Boynton Beach, Florida, USA. 0.1 to 0.35 and 0.05 to 0.20 of relative pressure (P/P0) adsorption data were used. Using the Barrett–Joyner–Halenda (BJH) method, the total pore volume and pore-size distributions were calculated for the relative pressure (P/P0) range of 0.01 to 0.95.

3. Results and discussions

3.1. HRSEM analysis of the single nanoparticles (ZnO, SiO$_2$) and the nanocomposites (ZnO/SiO$_2$)

Fig. 1 shows the HRSEM micrographs for the morphologies of the single nanoparticles (ZnO and SiO$_2$) and nanocomposites (ZnO/SiO$_2$) prepared at different mixing ratios (1:1, 1:2 and 2:1).

3.2. Particles size distribution of the nanocomposites (ZnO/SiO$_2$)

To study the particle size distribution of the nanocomposites synthesized, the imageJ software was used to determine the average particle size distribution and the results are shown in Fig. 2

As seen in Fig. 1, the morphology of the single ZnO (spherical shape) and SiO$_2$ (irregular shape) nanoparticles in (a) and (b), respectively, entirely change to a mixture of rod and nanoflower-like structures after the formation of the nanocomposites (ZnO/SiO$_2$). The morphological transformation may be due to the formation of oxide bands of Si–O–Zn, caused by the differences in the atomic radii of Si (0.4 Å) and Zn (0.74 Å) in the nanoparticles. Fig. 1(c), (d) and (e) suggest the formation of a new hybrid material of ZnO/SiO$_2$. It also noticed that as the amount of SiO$_2$ nanoparticles increase in the binary composite, the rate of agglomeration reduces (see Fig. 1(c), (d), and (e)). This indicates that the addition of SiO$_2$ nanoparticles could reduce the agglomeration of nanoparticles. The highly dispersed agglomerated rod-like morphology observed in Fig. 1(e) may be connected to the rise in dissolved Si or Zn concentration, which promotes the electrostatic force of attraction between the particles, resulting in the development of the fused rod-like shape in Fig. 1(c) and (d) [26]. The morphology of the ZnO/SiO$_2$ nanocomposites synthesized in this study is different from the irregular shape reported in [27] and the spherical shape reported in [28]. However, Is et al. [29] reported the effect of the concentration on the rough surfaces, and a nanoflower-like form of ZnO/SiO$_2$ nanocomposites. The difference between the morphologies may be linked to the method and the starting materials for the synthesis of the SiO$_2$ nanoparticles.

The average grain size was calculated using ImageJ software by deriving the corresponding grain diameter using optical micrographics. The result shows that the average grain sizes for the ZnO/SiO$_2$ nanocomposites prepared at mixing ratios of 1:1, 1:2 and 2:1 were 46.05, 42.75 and 40.34 nm, as shown in Fig. 2. This result confirmed that the ZnO/SiO$_2$ nanocomposites prepared at a mixing ratio of 2:1 have a smaller size compared to the others.

3.3. XRD analysis of the single nanoparticles (ZnO, SiO$_2$) and the nanocomposites (ZnO/SiO$_2$)

XRD was utilized to study the phase of ZnO, SiO$_2$ and the binary ZnO/SiO$_2$ nanocomposites produced with different mixing ratios. The results are given in Fig. 3.

The XRD pattern of the ZnO nanoparticles, shown in Fig. 3(a), demonstrates the existence of sharp diffraction peaks at 2 theta values of 21, 24, 26, 37, 46, 52, 56, 58, 59 and 62°, with the corresponding miller indices of (100), (002), (101), (102), (110), (103), (200), (112) and (004). The calculated lattice parameters for the synthesized ZnO nanoparticles were a = 3.240 Å c = 5.207 Å and V = 47.62 Å^3. This matches well with those in the JCPDS no 36-1541 for the hexagonal wurtzite phase of ZnO nanoparticles. Derikvandi et al. [30], Al-Ariki et al. [31] and Rezaei et al. [32] have reported similar miller indices for ZnO nanoparticles, with a similar phase of the ZnO nanoparticles. The absence of other peaks indicates the purity of the ZnO nanoparticles synthesized.

Using the Scherrer equation [33], the crystallite size of the ZnO nanoparticles was determined to be 31.52 nm. Fig. 3(b) shows the existence of diffraction peaks at 2θ values of 20, 26, 36, 39, 40, 42, 45, 50, 54, 56, 60, 63, 67 and 68°, corresponding to miller indices of (100), (101), (110), (012), (111), (200), (021), (112), (202), (103), (211), (212) and (301). These peaks matched perfectly to alpha quartz SiO$_2$, JCP2_83-0539; the absence of other diffraction peaks demonstrate a high degree of crystallinity of the synthesized SiO$_2$ nanoparticles from metakaolin. The synthetic SiO$_2$ nanoparticles made from kaolin had a crystallite size of 43.67 nm with lattice parameters of a = 4.921 Å, c = 5.416 Å and V = 113.590 Å^3. The XRD results for the ZnO/SiO$_2$ nanocomposites (1:2) in Fig. 3(d) show prominent diffraction peaks compared to the low intense peaks observed for the ZnO/SiO$_2$ nanocomposites prepared using the mixing ratios 1:1 and 2:1 (see Fig. 3(c) and (e), respectively). The high peak intensity in Fig. 3(d) may be linked to the increasing amount of SiO$_2$ in the nanocomposite (ZnO/SiO$_2$) which further enhanced the crystallinity of the ZnO/SiO$_2$ nanocomposite. This observation could also be attributed to the fact that SiO$_2$ is more energetically stable in the nanocomposites than ZnO. In comparison with the result presented for SiO$_2$ and ZnO in Fig. 3(a) and (b), it is obvious that the SiO$_2$ alpha quartz is the dominating phase of the formed ZnO/SiO$_2$ nanocomposites. Additionally, the phase of single SiO$_2$ and ZnO nanoparticles did not change after the successful immobilization of SiO$_2$ nanoparticles onto the core shell of the ZnO nanoparticles, with the exception that ZnO appears at a higher diffraction angle, suggesting that the lattice structure of the ZnO was distorted after the nanocomposites were formed. The dominant effect of SiO$_2$ in the ZnO/SiO$_2$ nanocomposites matrix suggests the diffusion of silicon (Si) ions onto the core–shell of the Zn ions, based on an ionic radius mechanism, Si^{4+} (0.26 Å) with a smaller ionic radius diffused faster and successfully compared to Zn^{2+} (0.74 Å), with a higher ionic radius. Bahrami and Karami's [34] investigation further supported the finding of this research that the ZnO phase was unaffected by the addition of SiO$_2$. The average crystallite sizes were found to be 21.24, 29.56 and 15.36 nm for 1:1, 1:2 and 2:1 ZnO/SiO$_2$ nanocomposites, respectively. At a smaller dosage of SiO$_2$ nanoparticles, the 1:1 sample (b) displays a bigger increase in the crystallite size. This is because adding SiO$_2$ causes the ZnO nanoparticle unit cell to contract, which leads to the creation of Si–O–Zn oxide clusters. Wang et al. [35] reported that this may also be attributed to the electron affinity of the Si ion, which is
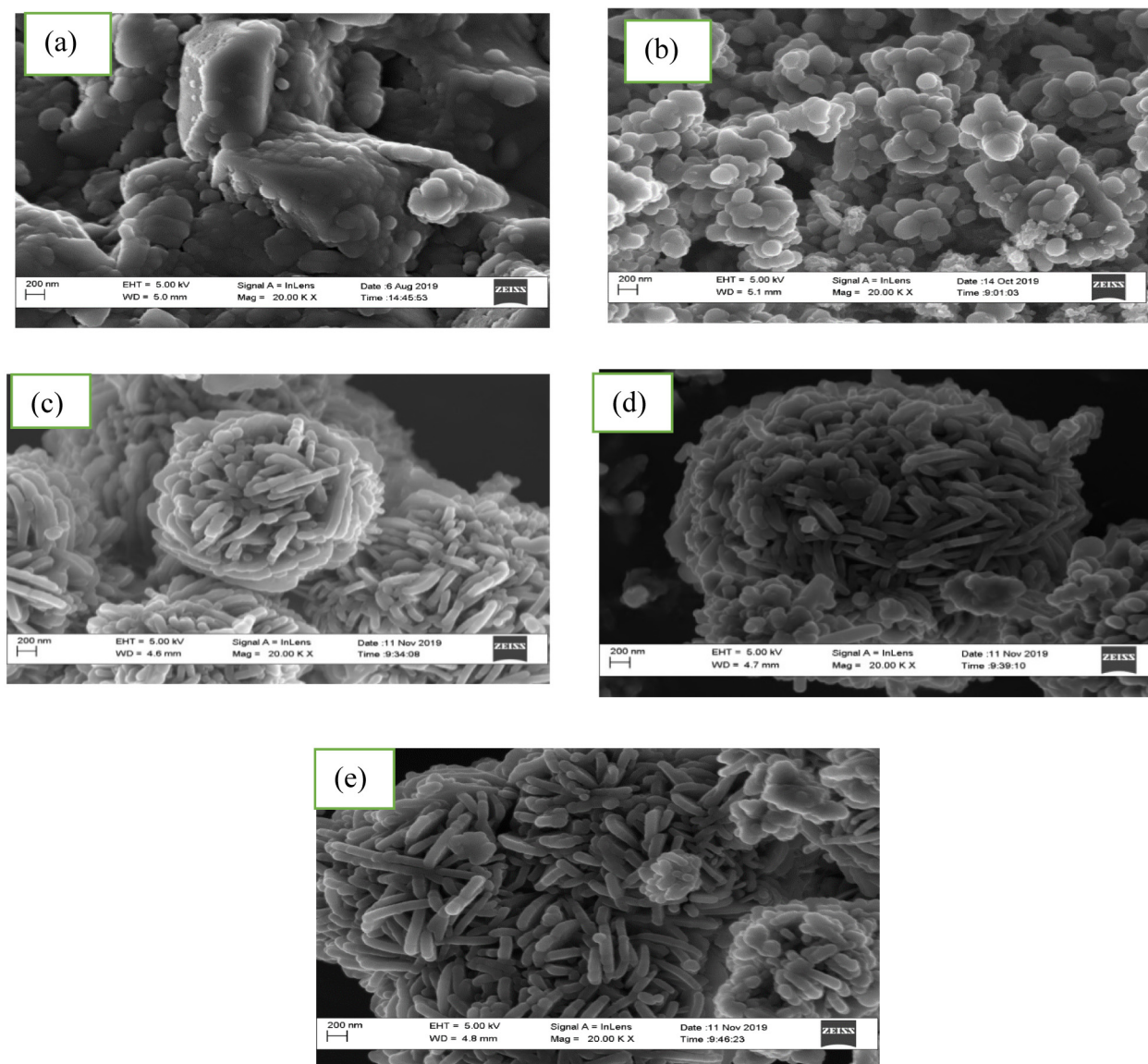
Fig. 1. HRSEM images of the (a) ZnO and (b) SiO$_2$ nanoparticles and the ZnO/SiO$_2$ nanocomposites with a mixing ratios of (c) 1:1 (d) (1:2) and (e) 2:1.

positive ($+134.068$ J mol^{-1}), compared to that of the Zn^{2+} ion (-58 J mol^{-1}); thus Zn^{2+} is more likely to interact with O^{-2} ($+140.976$ J mol^{-1}) than with the Si ion. The combination of the attractive/repulsive interactions improves the diffusivity of the oxygen and zinc ions in the domains and aids the movement of electrons within the molecules which caused the observed trend.

3.4. EDS analysis of the single nanoparticles (ZnO, SiO$_2$) and the nanocomposites (ZnO/SiO$_2$)

Fig. 4 displays the results of the EDX analysis used to evaluate the elemental composition of the ZnO/SiO$_2$ nanocomposites synthesized from ZnO and SiO$_2$ nanoparticles at different mixing ratios.

Fig. 4(a) reveals the presence of Zn, O and C. The O peak appears at 0.50 keV, whilst the peaks at 1.01, 8.65 and 9.49 keV correspond to the Zn ion, with an atomic percentage of 55.96%, whilst the O atomic percentage was 35.14% and the atomic percentage of C was 7.90%. The appearance of the peaks for carbon may be linked to the polyvinylpyrrolidone (PVP) used as stabilizing agent, surface stabilizer, nanoparticle dispersant,

structure directing agent and reducing agent for the synthesis of the ZnO nanoparticles. Fig. 4(b) confirms the existence of Si and O at 1.69 and 0.47 keV, respectively. The Si^{4+} ion percentage weight (wt%) was found to be between 45.47 and 52.18%. The produced ZnO/SiO$_2$ nanocomposites principally contain Si, Zn and O components, according to the EDS spectra in Fig. 4. O has a peak at 0.57 keV, Zn has peaks at 1.08, 8.75 and 9.68 keV, and Si has a peak at 1.75 keV. According to the results for the ZnO/SiO$_2$ nanocomposites, there is a rise in the binding energies for C, O, Zn and Si. This increase in binding energy may be caused by the diffusion of SiO$_2$ nanoparticles into the gaps between Zn^{2+} and O$_2$ ions. The Zn ion concentrations (wt. %) were found to be 55.09, 54.15 and 19.59% for (c), (d) and (e), respectively, while the Si ion concentrations (wt. %) were found to be 1, 1.87 and 40.49% for (c), (d) and (e), respectively. The increase in the atomic weight percentage of Si in the matrix of the ZnO/SiO$_2$ nanocomposites may be responsible for the formation of a highly compacted/fused rod-like network in Fig. 1(e). Moreover, the O ion concentrations (wt. %) were found to be 43.92, 43.98 and 34.91% for the samples displayed in Fig. 4(c), (d) and (e), respectively. This result corroborated the earlier results of XRD and the HRSEM in Fig. 3(d) and (e), where the XRD result of the sample with a higher dosage of
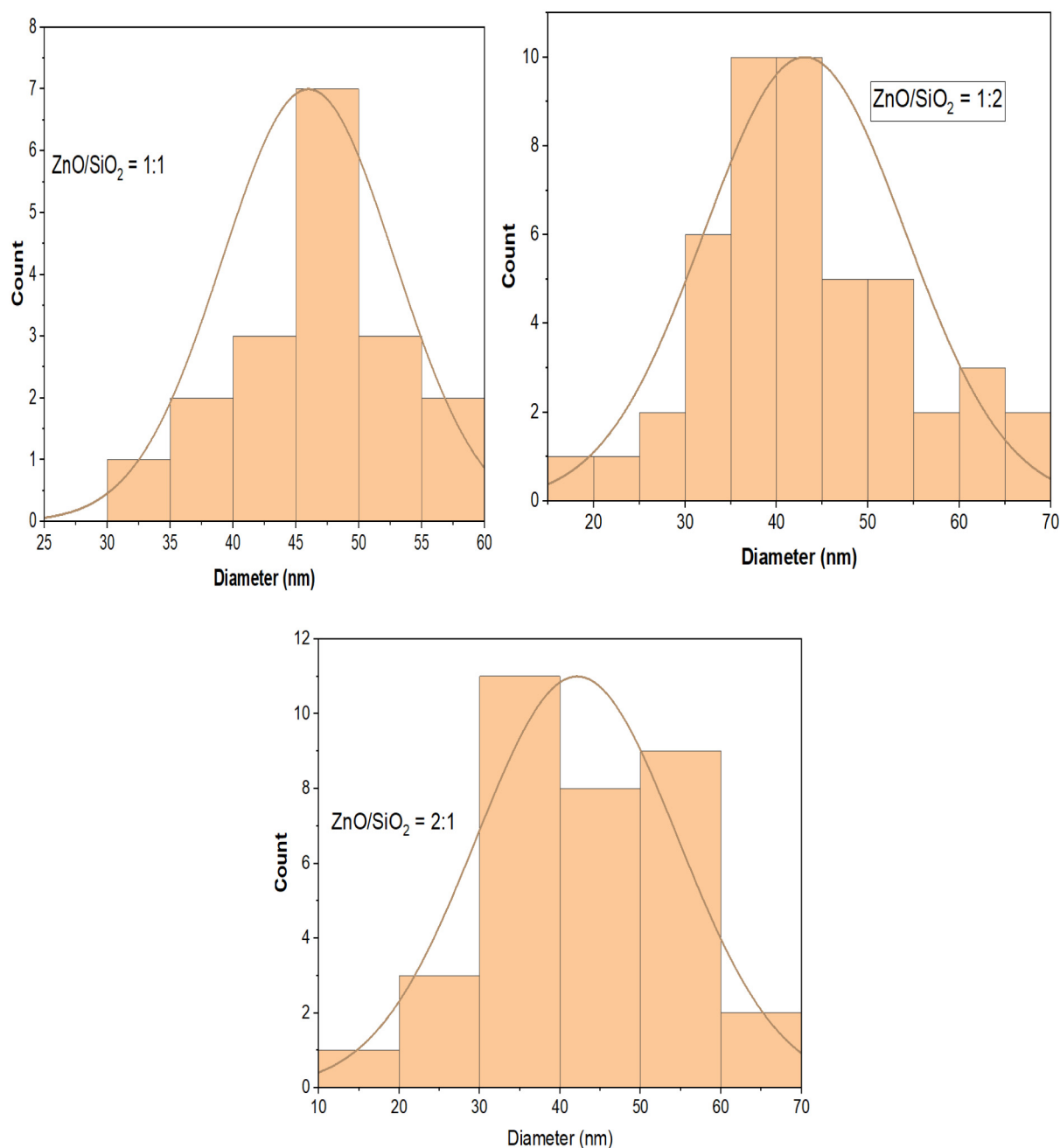
Fig. 2. Average grain sizes for the ZnO/SiO$_2$ nanocomposites prepared with mixing ratios of (a) 1:1, (b) 1:2 and (c) 2:1.

SiO$_2$ shows higher intense peaks and a larger particle size. The occurrence of both Zn, Si and oxygen in the EDS in Fig. 4(c), (d) and (e) is a confirmation that the ZnO/SiO$_2$ nanocomposites were formed.

3.5. Fourier transform infrared spectroscopy of the single nanoparticles (ZnO, SiO$_2$) and the nanocomposites (ZnO/SiO$_2$)

Fig. 5 shows the FTIR results for the single nanoparticles (ZnO and SiO$_2$) and the ZnO/SiO$_2$ nanocomposites prepared with different mixing ratios.

Fig. 5(a) shows adsorption bands at 1739 and 1358 cm^{-1}, which confirms the existence of C–H and C=O bonds [36]. The presence of a peak at 1024 cm^{-1} may be caused by the C-N stretching vibrations in the PVP utilized as a stabilizing agent for the production of the nanomaterials [37]. According to Nagaraju

et al. [38], the Zn–O bond can exhibit an FTIR absorption peak in the 500–400 cm^{-1} region. In this study, the Zn–O absorption peak is at 782 cm^{-1}, which confirmed the existence of the Zn–O bond [39]. This is different from the adsorption peak reported at 476 cm^{-1} for ZnO in Ref. [40]. The difference observed in this study may be ascribed to the calcination of the sample at 450 °C. SowriBabu et al. [41] have reported a similar trend, they found that a ZnO sample that had not been calcined initially displayed a Zn–O absorption peak at 457 cm^{-1}, which shifted to 518 and 682 cm^{-1} after being calcined at 300 and 500 °C, respectively. The adsorption peaks obtained in this analysis are greater than the 546 cm^{-1} reported by [42]. The PVP utilized as a stabilizing agent for the production of ZnO nanoparticles may be the cause of the difference observed.

The peaks at 793 and 1020 cm^{-1} in Fig. 5(b) are characteristic of the asymmetric vibration and symmetric stretching vibration
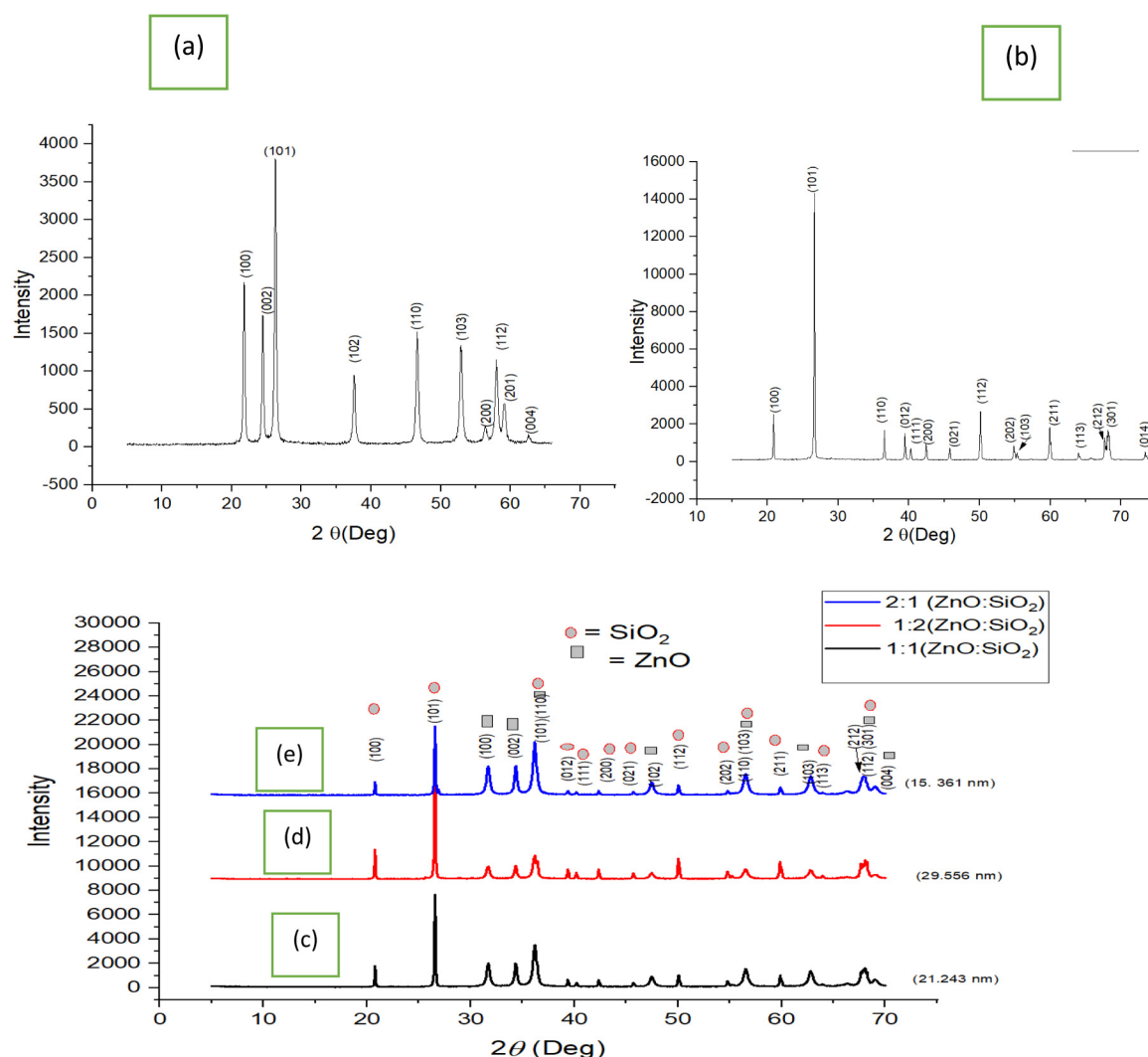
Fig. 3. XRD patterns of the ZnO (a) and SiO$_2$ nanoparticles and the (b) ZnO/SiO$_2$ nanocomposites with mixing ratios of (c) 1:1 (d) (1:2) and (e) 2:1.

of the O–Si–O bonds. The adsorption band visible at 950 cm^{-1} may be ascribed to the bond formed between silicon and hydrogen (Si–H). Fig. 5(c), (d) and (e) show similar adsorption bands for the ZnO/SiO$_2$ nanocomposites, irrespective of the mixing ratios, only that the frequencies for the ZnO and SiO$_2$ nanoparticles shifted to lower adsorption frequencies compared to the values obtained after the formation of the ZnO/SiO$_2$ nanocomposites (see Fig. 5(a) and (b)). This may be due to the interaction between the single nanoparticles (ZnO and SiO$_2$) in the ZnO/SiO$_2$ nanocomposites which collaborates with the analysis of [43] where the authors also stated that the adsorption frequency shifted to a lower frequency after the formation of composites. The bands at 1020 and 790 cm^{-1} were attributed to the asymmetric Si–O–Si stretching and bending vibrations in the ZnO/SiO$_2$ nanocomposites prepared with different mixing ratios. The presence of peaks relating to the Zn–O and Si–O bonds is evidence that the ZnO and SiO$_2$ nanoparticles in the nanocomposites interact strongly.

3.6. XPS analysis of the single nanoparticles (ZnO and SiO$_2$) and the ZnO/SiO$_2$ nanocomposites prepared with different mixing ratios

The results of the general XPS survey are shown in Fig. 6, which also shows the chemical states of the various elements found in the core shell of the single nanoparticles (ZnO, SiO$_2$) and ZnO/SiO$_2$ nanocomposites prepared with different mixing ratios.

Fig. 6 shows binding energies of 1047 and 1025.1 eV, respectively, corresponding to Zn 2p1/2 and Zn 2p3/2. This indicates the existence of Zn on the surfaces of the samples in the chemical state Zn^{2+}. The binding energy at 103.78 eV in Fig. 6(b), corroborates the idea that Si is present in the SiO$_2$ nanoparticles. The existence of C 1s at 285.6 eV in the XPS results may be as a result of the PVP utilized as a stabilizing agent for the synthesis of ZnO and ZnO/SiO$_2$.

3.7. XPS analysis of the Zn (2p3/2) orbital of the single nanoparticles (ZnO, SiO$_2$)

The XPS bands of Zn 2p3/2 for the ZnO nanoparticles and Si 2p for the SiO$_2$ nanoparticles were deconvoluted and Fig. 7 shows the results.

The binding energy at 1021.80 eV in Fig. 7(a) shows a single broad peak, which depicts the XPS spectrum of Zn 2p3/2 (ZnO). This further suggests that a strongly electropositive zinc ion (Zn^{2+}) is present in an electronegative environment charged with O^{2-} ions in the ZnO hexagonal Wurtzite structure geometry. This study is consistent with the observations made separately by Nguyen et al. [44] and Ferreira et al. [45], who found ZnO at binding energies of 1022.6 and 1022.15 eV. A large diffraction peak at 106.72 eV is observed in Fig. 7(b), which indicates the existence of silicon in the +4 oxidation state (Si^{4+}).
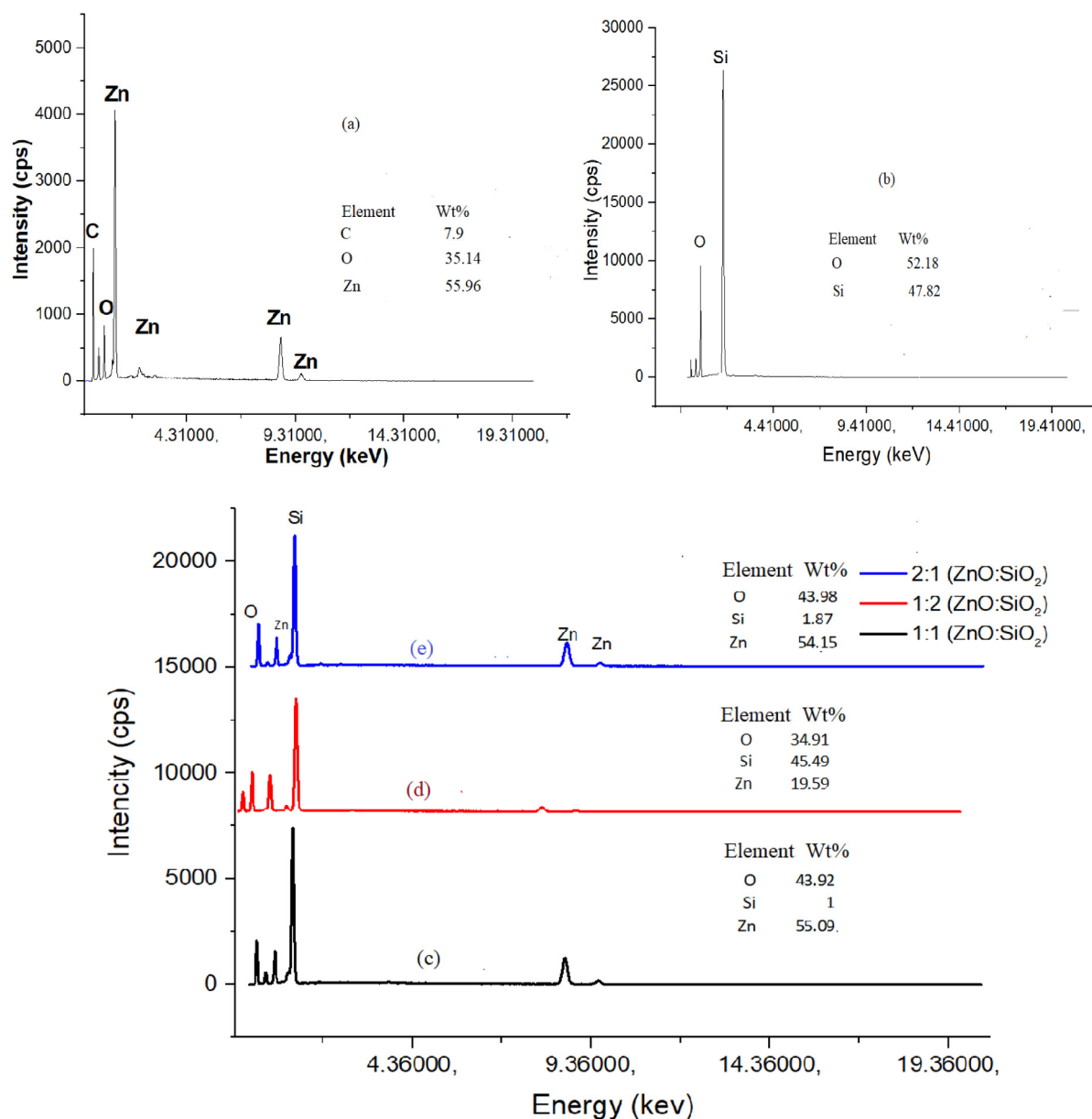
Fig. 4. EDS of the prepared (a) ZnO and (b) SiO$_2$ nanoparticles and the ZnO/SiO$_2$ nanocomposites with mixing ratios of (c) 1:1 (d) 1:2 and (e) 2:1.

3.8. XPS deconvoluted spectrum of O 1s for the ZnO and SiO$_2$ nanoparticles

XPS was used to study the deconvoluted O 1s spectra of the ZnO and SiO$_2$ nanoparticles and the results are presented in Fig. 8.

Three distinct peaks at 530.6, 532.2 and 533.5 eV for the binding energies correlating to O^{2-} and O$^-$ ions can be seen in Fig. 8(a). A peak, commonly referred to as the zinc oxide peak, appears at 530.6 eV, which is indicative of zinc oxide (ZnO). Wang et al. [46] reported that the O^{2-} ions in non-metallic oxides, such as ZnO nanoparticles, typically have a binding energy between 527 and 530 eV for O 1s [35]. The common binding energy for the atoms of oxygen present in the ZnO matrix is between 530.6 and 531.1 eV. The coordination of oxygen atoms, also known as O$^-$ ions, which form bonds like C=O and COO$^-$, may be the cause of the appearance of peaks at 531.1 and 532 eV [47]. The binding energies at 530 or 532 eV, match to ZnO, and the binding energies of 530.6, 532.2 and 533.2 eV, which were attributed to O^{2-}, O$^-$ ions and Zn–O, respectively, have also been reported by

another researcher. Likewise, Pawlak et al. [48] noticed a similar pattern, assigning O^{2-} and O$^-$ binding energies of 530.6 and 532.2 eV to O-Zn–O and Zn(OH)$_2$, respectively. The O 1s spectrum shown in Fig. 8(b) showed the existence of a single sharp peak at 536.3 eV. The existence of just one peak indicates the existence of oxygen atoms in the SiO$_2$ nanoparticles. Kamarulzaman et al. [49] reported a comparable finding in their research. The disparity between the results of this study and the values (532.3 eV) published by Lanco et al. [50] may be ascribed to the methods of production and the precursor (metakaolin) used for the produced SiO$_2$ in this study.

3.9. XPS analysis of the Zn and Si states in the nanocomposites (ZnO/SiO$_2$)

XPS was further used to study the chemical state of the Zn and Si in the ZnO/SiO$_2$ nanocomposites and the results of the deconvoluted XPS spectra of Zn and Si are presented in Fig. 9.
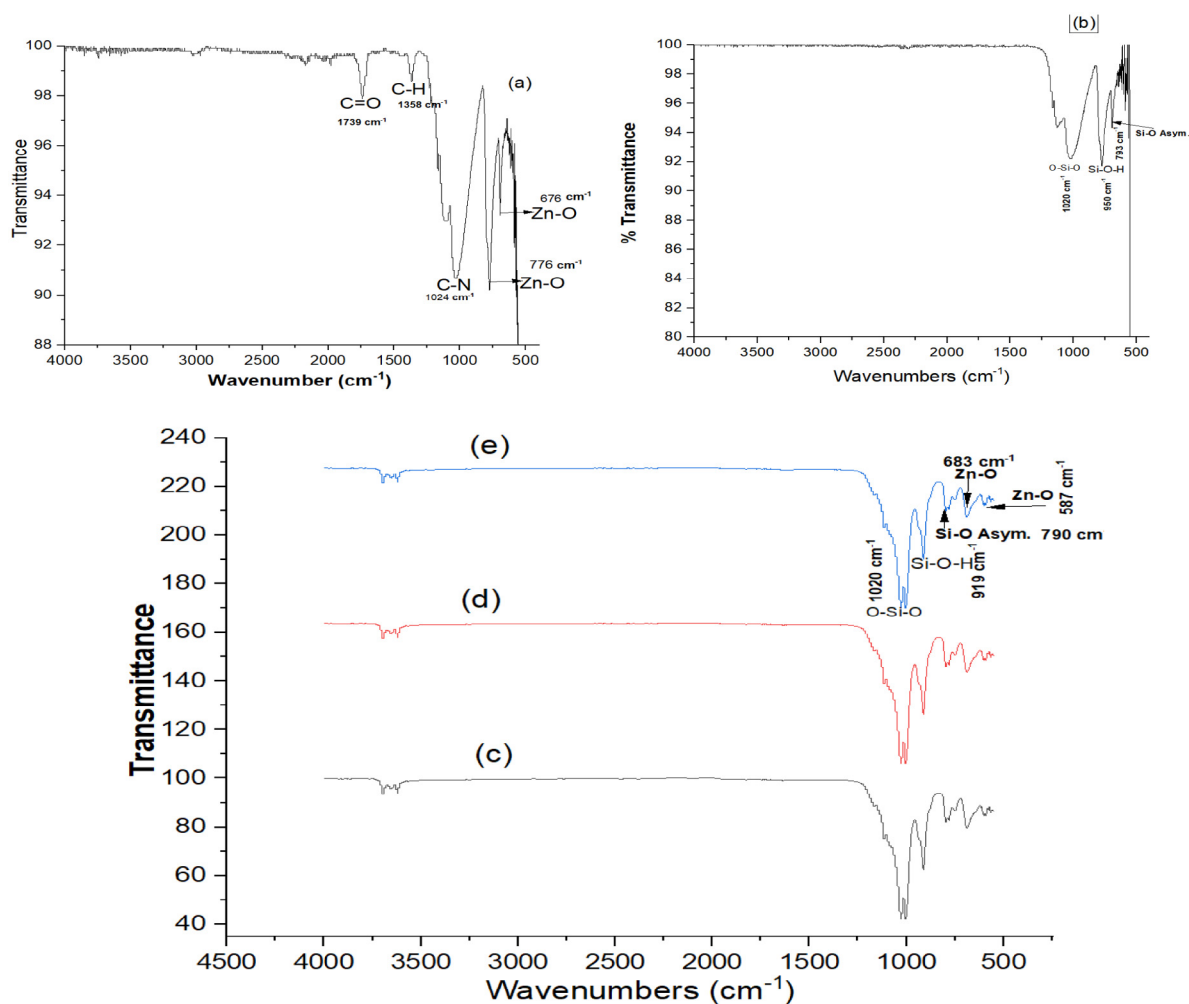
Fig. 5. FTIR plots for the (a) ZnO and (b) SiO$_2$ nanoparticles and the ZnO/SiO$_2$ nanocomposites with mixing ratios of (a) 1:1 (b) 1:2 and (c) 2:1.

The Zn element in the ZnO/SiO$_2$ nanocomposites likely exists in the $+1$ valence as opposed to Zn^{2+} noted earlier for the single ZnO nanoparticles. Fig. 9(a) shows peaks at 1045.63 and 1022.63 eV that correspond to the Zn 2p1/2 and Zn 2p3/2 orbitals (a). In the ZnO/SiO$_2$ nanocomposites, the existence of only $+1$ Zn ion suggests the creation of chemical bonds with other elements, which caused the spin–spin splitting of the Zn orbital, as seen in Fig. 9. (a). The XPS spectrum of Zn 2p in the ZnO/SiO$_2$ nanocomposites shows that the ZnO nanoparticles have been transformed and incorporated into SiO$_2$ to form the ZnO/SiO$_2$ nanocomposites. Fig. 9(b) indicates that after the development of the ZnO/SiO$_2$ nanocomposite, Si 2p3/2 remained unchanged. This result confirms the stability of the SiO$_2$ nanoparticles in the composites. Additionally, Si exists in the $+4$ oxidation state (Si^{4+}) in the composites.

3.10. Brunauer–Emmett–Teller (BET) of ZnO and SiO$_2$ nanoparticles and the ZnO/SiO$_2$ nanocomposites prepared with mixing ratios of 1:1, 1:2 and 2:1

The BET nitrogen adsorption–desorption isotherm was used to estimate properties (surface area, pore volume and pore diameter) for the individual nanoparticles (ZnO and SiO$_2$) and the corresponding ZnO/SiO$_2$ nanocomposites prepared with different mixing ratios, and the results are presented in Fig. 10 and Table 1.

The N$_2$ adsorption/desorption isotherms of the ZnO and SiO$_2$ nanoparticles and the ZnO/SiO$_2$ nanocomposites, as shown in

Table 1
The surface area, pore volume and pore diameter of the pure nanoparticles (ZnO and SiO$_2$) and the ZnO/SiO$_2$ nanocomposites.

Sample	Surface area (m^2/g)	Pore volume (cc/g)	Pore diameter (nm)
ZnO	8.620	0.353	26.173
SiO$_2$	0.386	0.002	32.150
ZnO/SiO$_2$ (1:1)	39.042	0.216	18.712
ZnO/SiO$_2$ (1:2)	55.602	0.296	13.135
ZnO/SiO$_2$ (2:1)	82.243	0.336	8.001

Table 1, demonstrate that the BET surface area for the single ZnO and SiO$_2$ nanoparticles were 8.620 and 0.386 m^2/g. After the synthesis of the ZnO/SiO$_2$ nanocomposite, the surface area increases, irrespective of the mixing ratio. The results indicate that the ZnO/SiO$_2$ nanocomposites synthesized using ZnO/SiO$_2$ in a 2:1 ratio recorded the highest surface area of 82.243 m^2/g, compared to 39.042 and 55.602 m^2/g recorded for the mixing ratios of 1:1 and 1:2, respectively. This result shows that the change in the surface area depends on the mixing ratios of the nanoparticles. These findings are very similar to those of the XRD data presented in Fig. 3, where the ZnO/SiO$_2$ nanocomposites synthesized at a mixing ratio of 2:1 had the smallest crystallite size compared to the other mixing ratios. This may be related to the high surface area recorded for the ZnO/SiO$_2$ nanoparticles prepared with the mixing ratio of 2:1. The observed trend in this respect is not suppressed because the smaller the crystallite size
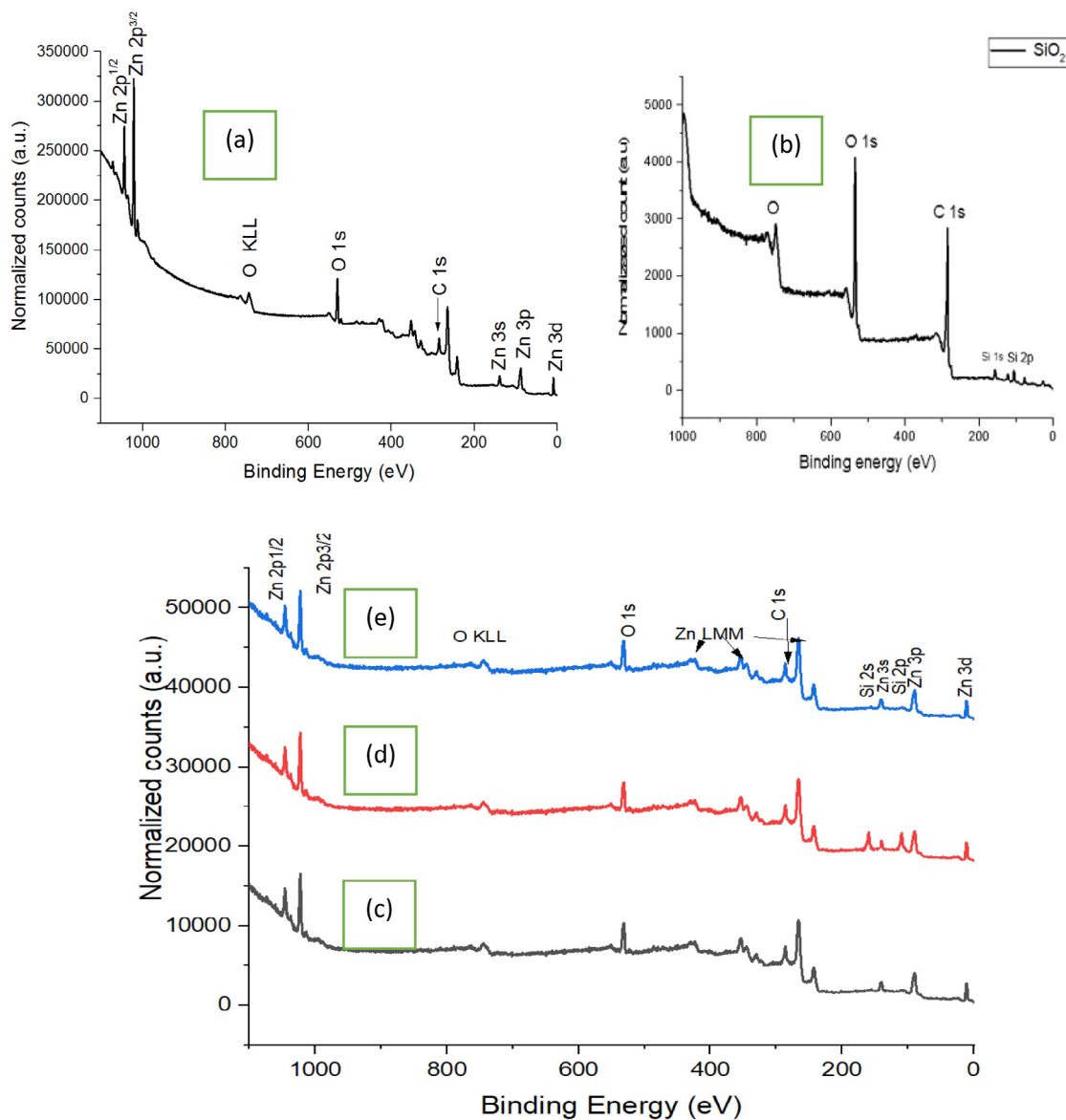
Fig. 6. XPS survey of (a) ZnO and (b) SiO$_2$ nanoparticles and the ZnO/SiO$_2$ nanocomposites with mixing ratios of (c) (1:1), (d) (1:2) and (c) (2:1).
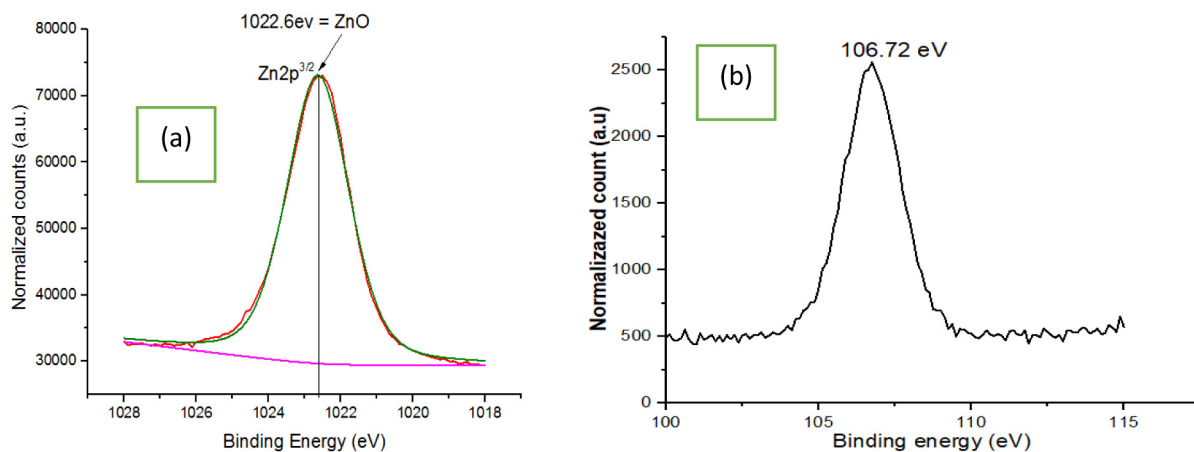

Fig. 7. (a) XPS spectra of Zn 2p3/2 for the ZnO nanoparticles and (b) Si 2p for the SiO$_2$ nanoparticles.
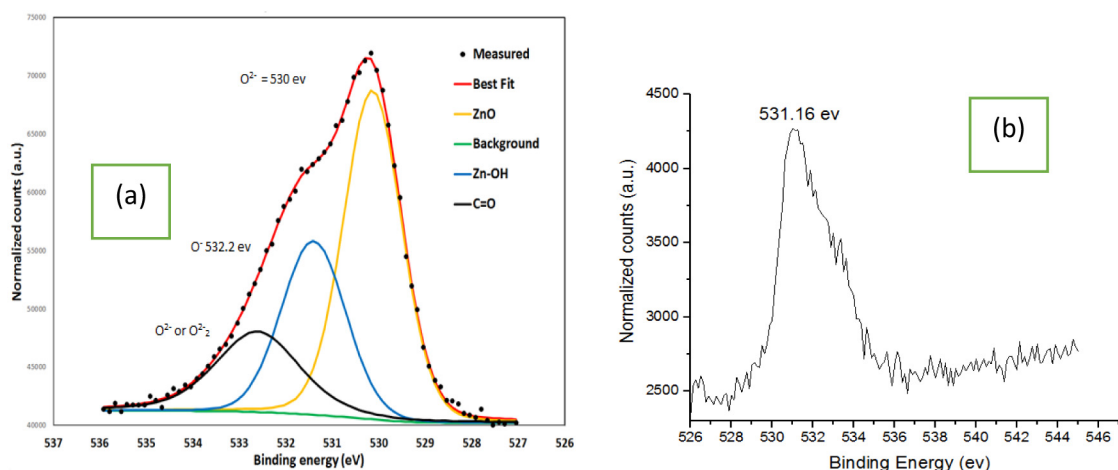
Fig. 8. Comparison of the orbital binding energy states of O 1s for (a) ZnO and (b) SiO$_2$ nanoparticles.
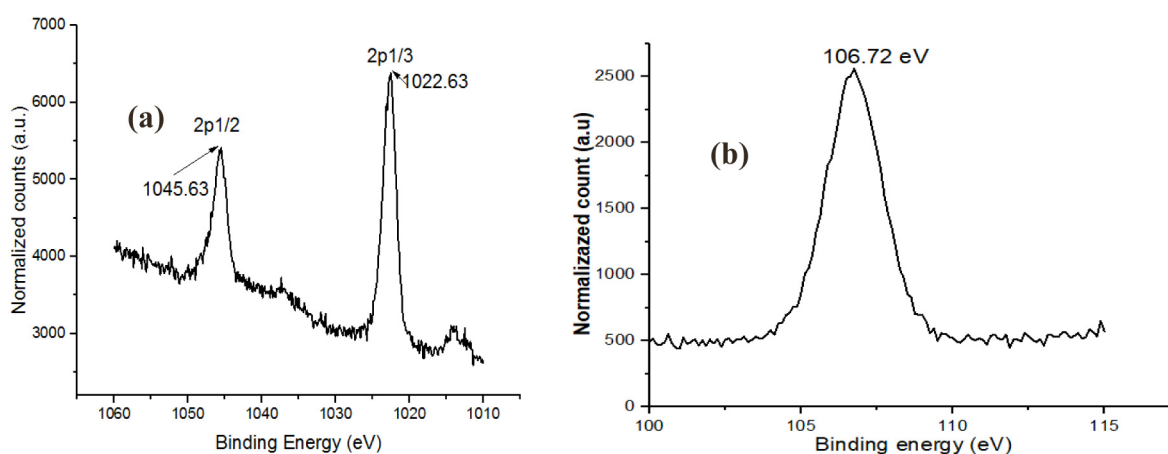

Fig. 9. XPS spectra of (a) Zn 2p3/2 and (b) Si 2p3/2 in the ZnO/SiO$_2$ nanocomposite.

of a material, the higher the surface area. [18] Additionally, the high surface area observed after the formation of the nanocomposites is an indication that more active sites were produced when the ZnO/SiO$_2$ nanocomposites was formed.

The high surface area could also be ascribed to the fact that the sol–gel process causes the ZnO and SiO$_2$ lattice structure to delaminate and cross-link, making the internal surface of the ZnO/SiO$_2$ accessible and increasing the specific surface area after the formation of the nanocomposites. This observed trend could be the reason why the pore size decreases as the surface area increases, as reported in Table 1: 32.150, 26.173, 18.712, 13.135, 8.001 nm for SiO$_2$, ZnO, ZnO/SiO$_2$ (1:1), ZnO/SiO$_2$ (1:2) and ZnO/SiO$_2$ (2:1) nanocomposites, respectively, indicating that the delaminated ZnO nanoparticles were distributed uniformly throughout the SiO$_2$ nanoparticle matrix. It is obvious from Table 1 that the surface area of the nanoparticles depends on the mixing ratio used for the formation of the ZnO/SiO$_2$ nanocomposites.

Based on these findings, it can be concluded that the ZnO/SiO$_2$ nanocomposites prepared using the mixing ratio of 2:1 have the potential to be employed for adsorption, catalysis, separation barrier, storage processes and drug delivery, since these processes rely on interface phenomena and benefit greatly from the use of high-surface-area materials and the intensification of these processes directly depend on the amount of surface area available for interactions. The findings in this research corroborate the findings of Zenkovets et al. [51] who synthesized silica/montmorillonite

nanocomposites and reported an increase in surface area after the formation of the nanocomposites.

Fig. 10 shows that the ZnO and SiO$_2$ nanoparticles and the ZnO/SiO$_2$ nanocomposites produced follow type IV isotherms and have residual rings at relative pressures of P/P$_0$ in the range 0.5 to 1, indicating monolayer adsorption [52]. According to the values of the pore diameter obtained for the SiO$_2$ and ZnO nanoparticles and the ZnO/SiO$_2$ (1:1), ZnO/SiO$_2$ (1:2) and ZnO/SiO$_2$ (2:1) nanocomposites, these indicate that the delaminated ZnO nanoparticles were distributed uniformly. According to the IUPAC standard, ZnO and SiO$_2$ nanoparticles and the ZnO/SiO$_2$ nanocomposites produced have a mesoporous structure since their pore diameters are between 2 and 50 nm [53].

3.11. Comparison of the findings from the current research with previous studies in the literature

The findings from this research have been compared with the results of previous research in the literature, as shown in Table 2

From Table 2, it is evident that many of the researchers that have carried out an analysis on the production of ZnO/SiO$_2$ nanoparticles and other composites of ZnO and SiO$_2$ nanoparticles with other materials, but did not vary the molar ratio of both materials as compared to this current research. This makes the current research unique because of the variation of the mixing ratio of both the nanoparticles (ZnO and SiO$_2$) used for the formation of the nanocomposites (ZnO/SiO$_2$). From the previous
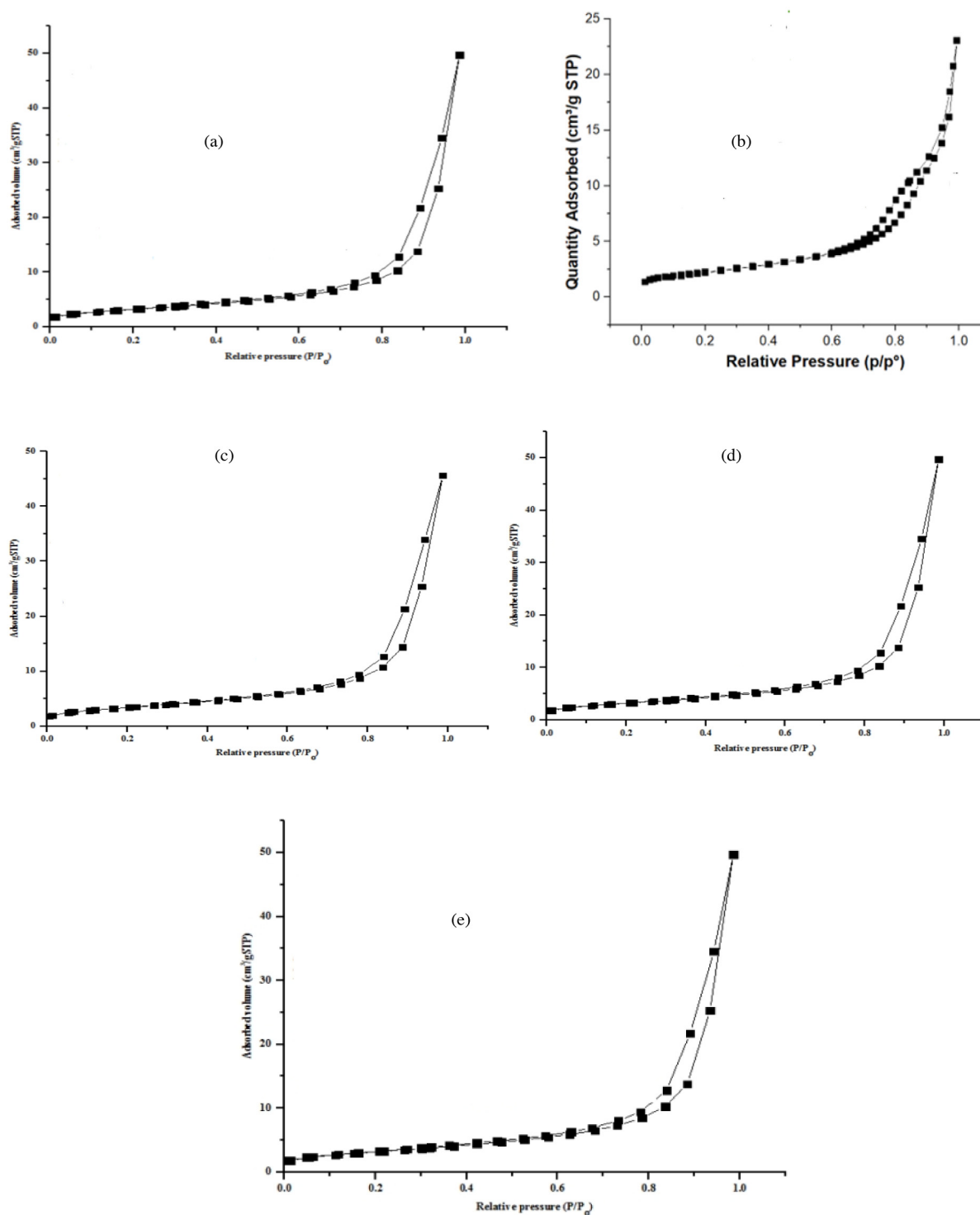
Fig. 10. BET Plots of ZnO (a) and SiO$_2$ (b) nanoparticles and the ZnO/SiO$_2$ nanocomposites prepared with mixing ratios of (c) 1:1, (d) 1:2 and (e) 2:1.

studies, it can be seen that the particles sizes obtained in this study (21, 29 and 15 nm for 1:1, 1:2 and 2:1 mixing ratios) are lower than the values recorded in the selected review and are comparable with the crystallite size reported by Lyu et al. [54] and Kazemzadeh [55]. This is an indication that the material used in this current study may have advanced potential compared to the others, especially in the area of treating wastewater and in the medical industries, since the use of the nanomaterials has been ascribed to the crystallite of the materials in these areas. Additionally, nanorods were synthesized in this current

study compared to spherical, flower and hazy-like structures reported in the previous studies. The differences observed in this study may be related to the different materials used and the use of naturally available material for the synthesis of the SiO$_2$ nanoparticles.

4. Conclusion

ZnO/SiO$_2$ nanocomposites with different mixing ratios of ZnO and SiO$_2$ nanoparticles (1:1, 1:2 and 2:1) were successfully

Table 2
Comparison of the results of the ZnO/SiO$_2$ nanocomposites with previous studies.

Nanomaterials	Method of Synthesis	Synthesis conditions	Crystallite size (nm)	Shape	Characterization tools	Mixing Ratio	Ref.
SiO$_2$/PVA and SiO$_2$/PMMA			14–20	hazy like	XRD, FT-IR, UV/visible	different proportions of 20 : 1, 10 : 1, and 5	[54]
TiO$_2$/SiO$_2$, Fe$_3$O$_4$/SiO$_2$	sol–gel	stirred for 24 h and aged at 100 °C for 24 h. Calcined for 3 h at 400 °C.	30, 25	Spherical	XRD, FESEMs, TEMs	1:01	[55]
Ag/ZnO	facile method	Stirred at 60 °C for 1h at and oven dry at 60 °C overnight	10–20	Spherical	SEM, EDS, TEM	2, 5 and 10 were selected to investigate the effect of Ag content	[56]
Ag–ZnO	Green method	Stirred at 70 °C and Calcined at 500 °C for 10 min	15 to 25 (TEM) 12 to 20 (XRD)	flower-like	XRD, FT-IR, XPS, SEM, TEM, XPS, UV– Vis	Change in concentration of Ag nanoparticles 2, 8, 10% and	[57]
Fe$_3$O$_4$/SiO$_2$		The solution was stirred for 5 h and centrifuged oven dried in a 100 °C	50, 43, 41		FTIR, XRD,	5, 15 and 30% SiO$_2$ concentrations	[58]
Ni-Ag		Stirred for 3 h, the solution was allowed to stand overnight at room temperature and dried for 4 h at 120 °C, calcined at 450 °C for 6 h	22, 19 and 26 for Ag-ZnO			Ni and Ag (0, 1, 3 and 5 mol.%) and ZnO was constant	[59]
ZnO/SiO$_2$	Sol–gel	Synthesized at room temperature, ageing for 48 calcination at 500 °C.	20.3	nanoflower-like	XRD, SEM, EDS FTIR, HRSEM, XPS	5, 10 and 20% of zinc oxide precursor solution	[60]
Chitosan/Fe$_3$O$_4$	Sol–gel		45 (Fe$_3$O$_4$) and 27	Spherical	DLS, FESEM, TEM, VSM, XPS, FT-IR, XRD	–	[61]
ZnO/SiO$_2$	Sol–gel	Stirred for 2 h,. oven-dry for 3 h at 130 °C.	34.09	irregular	SEM, XRD, BET, FT-IR	–	[24]
Ag-ZnO	In situ facile green	Temperature of 80 °C, and pH of 7–8	76.5, 75.8, 74.6 and 47.9	Spherical	XRD, ATR-FTIR, FESEM, TEM	1, 3, 5 and 8% of Ag	[62]
Chitosan-ZnO	Sol–gel	Stirred for 24 h, dried during 20 h at 60 °C	45.3	–	FTIR, XRD, TGA	Percent of ZnO (5, 10, 15 and 20 wt%)	[63]

synthesized using the sol–gel and wet impregnation methods. The morphology, crystallite size, elemental compositions, functional groups and chemical state of the ZnO, SiO$_2$ nanoparticles and ZnO/SiO$_2$ nanocomposites synthesized were determined by HRSEM, EDS, XRD, FT-IR and XPS, respectively. The HRSEM analysis showed that the morphology of the ZnO/SiO$_2$ nanocomposites synthesized was greatly affected by the amount of SiO$_2$ nanoparticles in the composite matrix. The ZnO/SiO$_2$ nanocomposite synthesize using a mixing ratio of 2:1 was found to be less agglomerated compared to the ZnO/SiO$_2$ nanocomposites synthesize using 1:1 and 1:2 ratios of ZnO and SiO$_2$ nanoparticles. The crystallite size, morphology, particle size distribution, surface area, elemental composition and chemical state of the ZnO/SiO$_2$ nanocomposites synthesized are affected by the mixing ratio. The ZnO/SiO$_2$ nanocomposites prepared using a 2:1 mixing ratio have better physicochemical properties compared to the individual nanoparticles and the other ZnO/SiO$_2$ nanocomposites. The ZnO/SiO$_2$ nanocomposite prepared at a 2:1 mixing ratio had a smaller crystallite size (15.36 nm.) and higher surface area (82.243 m^2/g). According to the findings from this research, it can be said that the nanocomposites produced using the ratio of 2:1 of ZnO and SiO$_2$ nanoparticles have superior properties compared to the others. Therefore, ZnO/SiO$_2$ nanocomposite prepared using a mixing ratio of 2:1 for the ZnO and SiO$_2$ nanoparticles can be applied in different fields, such as construction, catalyst and adsorbent in the treatment of wastewater due to its lesser agglomeration.

CRediT authorship contribution statement

Elijah Yanda Shaba: Conception and design of study, Material preparation, data collection and analysis, Writing – original draft. **Jimoh Oladejo Tijani:** Conception and design of study, Material preparation, data collection and analysis, Project administration, Resources, Software. **John Olusanya Jacob:** Conception and design of study, Material preparation, data collection and analysis, Design and validation of the methodology, Writing – review & editing. **Mohammed Abubakar Tanko Suleiman:** Conception and design of study, Material preparation, data collection and analysis, Supervision.

Declaration of competing interest

The authors have no relevant financial or non-financial interests to disclose

Data availability

Data will be made available on request.

References

[1] S.H. Nile, V. Baskar, D. Selvaraj, A. Nile, J. Xiao, G. Kai, Nanotechnologies in food science: Applications, recent trends, and future perspectives, Nano-Micro Lett. 12 (1) (2020) 1–34, http://dx.doi.org/10.1007/s40820-020-0383-9.

[2] Michele Iafisco, V.P. Suresh Kumar, N. Manikandan, N. Nagaprasad, Jule LetaTesfaye, Ramasamy Krishnaraj, Analysis of the performance characteristics of ZnO nanoparticles' dispersed polyester oil, Adv. Mater. Sci. Eng. (2022) 1–10, http://dx.doi.org/10.1155/2022/4844979.

[3] A. Spoială, C.I. Ilie, C.R.D. Truşcă, O.C. Oprea, V.A. Surdu, B.S. Vasile, A. Ficai, D. Ficai, E. Andronescu, L.M. Diţu, Zinc oxide nanoparticles for water purification, Materials (Basel) 14 (2021) 1–15, http://dx.doi.org/10.3390/ma14164747.

[4] C. Pushpalatha, J. Suresh, V.S. Gayathri, S.V. Sowmya, D. Augustine, A. Alamoudi, B. Zidane, A.N.H. Mohammad, S. Patil, Zinc oxide nanoparticles: a review on its applications in dentistry, Front. Bioeng. Biotechnol. 10 (2022) 1–9, http://dx.doi.org/10.3389/fbioe.2022.917990.

[5] T. Strachowski, M. Baran, M. Małek, R. Kosturek, E. Grzanka, J. Mizeracki, A. Romanowska, S. Marynowicz, Hydrothermal synthesis of zinc oxide nanoparticles using different chemical reaction stimulation methods and their influence on process kinetics, Materials 15 (2022) 1–12, http://dx.doi.org/10.3390/ma15217661.

[6] A. Ali, A.R. Phull, M. Zia, Elemental zinc to zinc nanoparticles: is ZnONPS crucial for life? Synthesis, toxicological and environmental concerns, Nanotechnol. Rev. 7 (2018) 413–441, http://dx.doi.org/10.1515/ntrev-2018-0067.

[7] F. Islam, S. Shohag, M.J. Uddin, M.R. Islam, H.M. Nafady, A. Akter, S. Mitra, A. Roy, T.B. Emran, S. Cavalu, Exploring the journey of zinc oxide nanoparticles (ZnONPS) toward biomedical applications, Materials 15 (2022) 1–19, http://dx.doi.org/10.3390/ma15062160.

[8] S. Ghattavi, A. Nezamzadeh-Ejhieh, A double-Z-scheme ZnO/AgI/WO$_3$ photocatalyst with high visible light activity: Experimental design and mechanism pathway in the degradation of methylene blue, J. Mol. Liq. (2020) 1–14, http://dx.doi.org/10.1016/j.molliq.2020.114563.

[9] A. Norouzi, A. Nezamzadeh-Ejhieh, Investigation of the simultaneous interactions of experimental variables and mechanism pathway in the photodegradation of methylene blue by binary ZnO/Cu$_2$O photocatalyst, Mater. Res. Bull. 164 (2023) 112237, http://dx.doi.org/10.1016/j.materresbull.2023.112237.

[10] Z. Khodami, A. Nezamzadeh-Ejhieh, Investigation of photocatalytic effect of ZnO–SnO$_2$/nano clinoptilolite system in the photodegradation of aqueous mixture of 4-methylbenzoic acid/2-chloro-5-nitrobenzoic acid, J. Mol. Catal. A 409 (2015) 59–68, http://dx.doi.org/10.1016/j.molcata.2015.08.013.

[11] A. Shirzadi, A. Nezamzadeh-Ejhieh, Enhanced photocatalytic activity of supported CuO–ZnO semiconductors towards the photodegradation of mefenamic acid aqueous solution as a semi real sample, J. Mol. Catal. A 411 (2016) 222–229, http://dx.doi.org/10.1016/j.molcata.2015.10.027.

[12] P. Singh, S. Srivastava, S.K.K. Singh, Nanosilica: Recent progress in synthesis, functionalization, biocompatibility and biomedical applications, ACS Biomater. Sci. Eng. 5 (2019) 4882–4898, http://dx.doi.org/10.1021/acsbiomaterials.9b004.

[13] E.Y. Shaba, J.O. Jacob, J.O. Tijani, M.A.T. Suleiman, A critical review of synthesis parameters affecting the properties of zinc oxide nanoparticle and its application in wastewater treatment, Appl. Water Sci. 11 (2021) 1–48, http://dx.doi.org/10.1007/s13201-021-01370-z.

[14] K.S. Rao, K. El-Hami, T. Kodaki, K. Matsushige, K. Makino, A novel method for synthesis of silica nanoparticles, J. Colloid Interface Sci. 1 (2005) 125–131, http://dx.doi.org/10.1016/j.jcis.2005.02.019, PMID: 15913636.

[15] S. Prabha, D. Durgalakshmi, S. Rajendran, E. Lichtfouse, Plant-derived silica nanoparticles and composites for biosensors, bioimaging, drug delivery and supercapacitors: a review, Environ. Chem. Lett. 19 (2020) 1667–1691, http://dx.doi.org/10.1007/s10311-020-01123-5.

[16] E. Akhayere, D. Kavaz, A. Vaseashta, Efficacy studies of silica nanoparticles synthesized using agricultural waste for mitigating waterborne contaminants, Appl. Sci. 12 (2022) 1–19, http://dx.doi.org/10.3390/app12189279.

[17] Z. Zidi, M. Ltifi, I. Zafar, Synthesis and attributes of nano-SiO$_2$ local metakaolin based-geopolymer, J. Build. Eng. 33 (2021) 101586, http://dx.doi.org/10.1016/j.jobe.2020.101586.

[18] J.O. Tijani, M.T. Bankole, A. Hussein, J.A. Oketoye, A.S. Abdulkareem, Influence of synthesis parameters in the preparation of silicon (IV) oxide nanoparticles from dealuminated metakaolin and metakaolin with Na$_2$SiO$_3$, J. Chem Soc. Nigeria 44 (2019) 1143–1156.

[19] N. Baig, I. Kammakakam, W. Falath, Nanomaterials: a review of synthesis methods, properties, recent progress, and challenges, Mater. Adv. 2 (6) (2021) 1821–1871, http://dx.doi.org/10.1016/j.nanoso.2021.100728.

[20] I. Khan, K. Saeed, I. Khan, Nanoparticles: Properties, applications and toxicities, Arab. J. Chem. (2017) 1–24, http://dx.doi.org/10.1016/j.arabjc.2017.05.011.

[21] E.Y. Shaba, J.O. Tijani, J.O. Jacob, M.A.T. Suleiman, Simultaneous removal of Cu(II) and Cr(VI) ions from petroleum refinery wastewater using ZnO/Fe$_3$O$_4$ nanocomposite, J. Environ. Sci. Health A. Tox. Hazard. Subst. Environ. Eng. 57 (2022) 1146–1167, http://dx.doi.org/10.1080/10934529.2022.2162794.

[22] S. Ibsen, A. Sonnenberg, C. Schutt, R. Mukthavaram, Y. Yeh, I. Ortac, S. Manouchehri, S. Kesari, S. Esener, M.J. Heller, Recovery of drug delivery nanoparticles from human plasma using an electrokinetic platform technology, Small 11 (38) (2015) 5088–5096, http://dx.doi.org/10.1002/smll.201500892.

[23] E.Y. Shaba, J.O. Tijani, J.O. Jacob, M.A.T. Suleiman, Adsorptive potential of ZnOSiO$_2$ nanorods prepared via the sol–gel method for the removal of Pb(II) and Cd(II) from petroleum refinery wastewater, J. Chem. Technol. Biotechnol. 19 (2022) 2196–2217, http://dx.doi.org/10.1002/jctb.7098.

[24] M. Justine, J.H. Prabu, I. Johnson, A.R.D. Magimai, S.S. John, K. Kaviyarasu, Synthesis and characterization studies of ZnO and ZnO-SiO$_2$ nanocomposite for biodiesel applications, Mater. Today: Proc. 36 (2020) 440–446, http://dx.doi.org/10.1016/j.matpr.2020.05.0341-7.

[25] I.R. Fida', Y.W. Fen, M.F. Anuar, N.A.S. Omar, M.H.M. Zaid, K.A. Matori, R.E.M. Khaidir, Synthesis and characterization of ZnO-SiO$_2$ composite using oil palm empty fruit bunch as a potential silica source, Molecules 26 (2021) 1–11, http://dx.doi.org/10.3390/molecules26041061.

[26] B. Shrestha, L. Wang, H. Zhang, C.Y. Hung, L. Tangz, Gold nanoparticles mediated drug-gene combinational therapy for breast cancer treatment, Int. J. Nanomed. 15 (2020) 8109–8119, http://dx.doi.org/10.2147/IJN.S258625.

[27] V.L. Chandraboss, B. Karthikeyan, J. Kamalakkannan, S. Prabha, S. Senthilvelan, Sol-gel synthesis of TiO$_2$/SiO$_2$ and ZnO/SiO$_2$ composite films and evaluation of their photocatalytic activity towards methyl, Green J. Nanoparticles (2013) 1–7, http://dx.doi.org/10.1155/2013/507161.

[28] N.A. Al-Tayyar, A.M. Youssef, R.R. Al-Hindi, Antimicrobial packaging efficiency of ZnO-SiO$_2$ nanocomposites infused into PVA/CS film for enhancing the shelf life of food products, Food Packag. Shelf Life 25 (2020) 100523, http://dx.doi.org/10.1016/j.fpsl.2020.100523.

[29] F. Is, G. Fadillah, I. Sahroni, A. Kamari, S. Sagadevan, R.A. Doong, Nanoflower-like composites of ZnO/SiO$_2$ synthesized using bamboo leaves ash as reusable photocatalyst, Arab. J. Chem. 14 (3) (2021) http://dx.doi.org/10.1016/j.arabjc.2020.102973.

[30] H. Derikvandi, A. Nezamzadeh-Ejhieh, A comprehensive study on electrochemical and photocatalytic activity of SnO$_2$-ZnO/clinoptilolite nanoparticles, J. Mol. Catal. A 426 (2017) 158–169, http://dx.doi.org/10.1016/j.molcata.2016.11.011.

[31] S. Al-Ariki, N.A.A. Yahya, S.A. Al-A'nsi, M.H.H. Jumali, A.N. Jannah, R. Abd-Shukor, Synthesis and comparative study on the structural and optical properties of ZnO doped with Ni and Ag nanopowders fabricated by sol–gel technique, Sci. Rep. 11 (2021) 1–11, http://dx.doi.org/10.1038/s41598-021-91439-1.

[32] M. Rezaei, A. Nezamzadeh-Ejhieha, The ZnO-NiO nano-composite: A brief characterization, kinetic and thermodynamic study and study the arrhenius model on the sulfasalazine photodegradation, Int. J. Hydrog. Energy 45 (2020) 24749–24764, http://dx.doi.org/10.1016/j.ijhydene.2020.06.258.

[33] K.L. Seneviratnea, I. Munaweera, S.E. Peirisa, C.N. Peirisa, N. Kottegoda, Recent progress in visible-light active (VLA) TiO$_2$ nano-structures for enhanced photocatalytic activity (PCA) and antibacterial properties: A review, Iran. J. Catal. 11 (3) (2021) 217–245.

[34] K. Bahrami, Z. Karami, Core/shell structured ZnO@SiO$_2$-TTIP composite nanoparticles as an effective catalyst for the synthesis of 2-substituted benzimidazoles and benzothiazoles, J. Exp. Nanosci. 13 (1) (2018) 272–283, http://dx.doi.org/10.1080/17458080.2018.1542511.

[35] P.R. Wang, S. Mandal, H. Panigrahi, P. Das, K.K. Dinesh, Carbon dots: Fluorescence active, covalently conjugated and strong reinforcing nanofiller for polymer latex, Nano-Struct. Nano-Obj. 23 (2020) 1–9, http://dx.doi.org/10.1016/j.nanoso.2020.100477.

[36] M.L.B. Domingues, J.R. Bocca, S.L. Fávaro, E. Radovanovic, Disposable coffee capsules as a source of recycled polypropylene, Polímeros: Ciência e Tecnol. 30 (2020) 1–9, http://dx.doi.org/10.1590/0104-%201428.05518.

[37] K.I. Hadjiivanov, D.A. Panayotov, M.Y. Mihaylov, E.Z. Ivanova, K.K. Chakarova, S.M. Andonova, N.L. Drenchev, Power of infrared and Raman spectroscopies to characterize metal-organic frameworks and investigate their interaction with guest molecules, Chem. Rev. 121 (2020) 1286–1424, http://dx.doi.org/10.1021/acs.chemrev.0c0048.

[38] G. Nagaraju, S. Udayabhanu, S.A. Prashanth, M. Shastri, K.V. Yathish, C. Anupama, D. Rangappa, Electrochemical heavy metal detection, photocatalytic, photoluminescence, biodiesel production and antibacterial activities of Ag–ZnO nanomaterial, Mater. Res. Bull. 94 (2017) 54–63.

[39] J. Singhb, S. Kaur, G. Kaur, S. Basu, S.M. Rawat, Biogenic ZnO nanoparticles: a study of blueshift of optical band gap and photocatalytic degradation of reactive yellow 186 dye under direct sunlight, Green Process. Synth. 8 (2019) 272–280, http://dx.doi.org/10.1515/gps-2018-0084.

[40] F. Iazdani, A. Nezamzadeh-Ejhieh, The photocatalytic rate of ZnO supported onto natural zeolite nanoparticles in the photodegradation of an aromatic amine, Environ. Sci. Pollut. Res. (2021) http://dx.doi.org/10.1007/s11356-021-14544-8.

[41] K. Sowribabu, R.A. Ramachandra, C. Sujatha, K.R. Venugopal, A.N. Mallika, Synthesis and optical characterization of porous ZnO, J. Adv. Ceram. 2 (2013) 260–265.

[42] V.T. Salunke, P.B. Buchade, A.D. Shaligram, R.Y. Borse, FTIR study of ZnO powder prepared by self-combustion method at different temperature, World J. Adv. Res. Rev. 10 (2021) 277–280, http://dx.doi.org/10.30574/wjarr.2021.10.3.0237.

[43] S. Yasmeen, K.K. Mrinal, S. Badhan, Q. Rakibul, M.G. Abdul, M.M. Shah, Chromium (VI) ions removal from tannery effluent using chitosan-microcrystalline cellulose composite as adsorbent, Int. Res. J. Pure Appl. Chem. 10 (2016) 1–14, http://dx.doi.org/10.9734/IRJPAC/2016/23315.

[44] N.T. Nguyen, N.T. Nguyen, V.A. Nguyen, In situ synthesis and characterization of ZnO/chitosan nanocomposite as an adsorbent for removal of Congo red from aqueous solution, Adv. Polym. Technol. (2020) 1–8, http://dx.doi.org/10.1155/2020/3892694.

[45] F.C. Ferreira, W. Franceschi, B.R.C. Menezes, A.F. Biagioni, A.R. Coutinho, L.S. Cividanes, Synthesis, characterization, and applications of carbon nanotubes. carbon-based nanofillers and their rubber, Nanocomposites (2019) 1–45, http://dx.doi.org/10.1016/B978-0-12-813248-7.00001-8.

[46] T. Wang, B. Jin, Z. Jiao, G. Lu, J. Ye, Y. Bi, Photo-directed growth of Au nanowires on ZnO arrays for enhancing photoelectrochemical performances, J. Mater. Chem. A 2 (2014) 15553–15559, http://dx.doi.org/10.1039/c4ta02960g.

[47] E.H. Mohamed, F. Salah, M.H. Shawk, Preparation of modified nanoparticles of zinc oxide for removal of organic and inorganic pollutant, Trends Appl. Sci. Res. 12 (2017) 1–9, http://dx.doi.org/10.3923/tasr.2017.1.9.

[48] D.A. Pawlak, M. Ito, M. Oku, K. Shimamura, T. Fukuda, Interpretation of XPS O (1s) in mixed oxides proved on mixed perovskite crystals, J. Phys. Chem. B 106 (2020) 504–507, http://dx.doi.org/10.1021/jp012040a.

[49] N. Kamarulzaman, M.F. Kasim, N.F. Chayed, Elucidation of the highest valence band and lowest conduction band shifts using XPS for ZnO and Zn 0.99 Cu 0.01 o band gap changes, Results Phys. 6 (2016) 217–230, http://dx.doi.org/10.1016/j.rinp.2016.04.001.

[50] M.V. Lanco, V. Renman, J. Zhu, Optimizing carbon coating parameters for obtaining SiO_2/C anodes with improved electrochemical performance, J. Solid State Electrochem. 25 (2021) 1339–1351, http://dx.doi.org/10.1007/s10008-021-04912-2.

[51] G.A. Zenkovets, A.A. Shutilov, V.M. Bondareva, V.I. Sobolev, A. Marchuk, S.V. Tsybulya, I.P. Prosvirin, A. Ishchenko, V.Y. Gavrilov, New multicomponent $MoVSbNbCeO_x$/SiO_2 catalyst with enhanced catalytic activity for oxidative dehydrogenation of ethane to ethylene, Chem. Cat. Chem. (2020) 4149–4159, http://dx.doi.org/10.1002/cctc.202000489.

[52] J. Jiang, J. Cao, W. Wang, C. Mei, Analysis on the influence of component ratio on properties of silica/montmorillonite nanocomposites, Materials (Basel) 11 (2018) 1–12, http://dx.doi.org/10.3390/ma11112074, PMID: 30352956; PMCID: PMC6266273.

[53] J. Kermani, S. Mollazadeh, S. Kargozar, J. Vahdati Khakhi, Solution combustion synthesis (SCS) of theranostic ions doped biphasic calcium phosphates; kinetic of ions release in simulated body fluid (SBF) and reactive oxygen species (ROS) generation, Mater. Sci. Eng. C 118 (2021) 111533.

[54] W. Lyu, J. Wu, W. Zhang, Y. Liu, M. Yu, Y. Zhao, J. Feng, W. Yan, Easy separated 3D hierarchical coral-like magnetic polyaniline adsorbent with enhanced performance in adsorption and reduction of Cr(VI) and immobilization of Cr(III), Chem. Eng. J. 363 (2019) 107–119, http://dx.doi.org/10.1016/j.cej.2019.01.109.

[55] Y. Kazemzadeh, M. Sharifi, M. Riazi, R. Rezvani, M. Tabaei, Potential effects of metal oxide/SiO_2 nanocomposites in EOR processes at different pressures, Colloids Surf. A Physicochem. Eng. Asp. 559 (2018) 372–384, http://dx.doi.org/10.1016/j.colsurfa.2018.09.06.

[56] E.A. Alzahrani, A. Nabi, M.R. Kamli, S.M. Albukhari, S.A. Althabaiti, S.A. Al-Harbi, I. Khan, M.A. Malik, Facile green synthesis of ZnO NPs and plasmonic Ag-supported ZnO nanocomposite for photocatalytic degradation of methylene blue, Water 15 (2023) 384, http://dx.doi.org/10.3390/w15030384.

[57] F. Alharthi, A.A. Abdulaziz, S.A. Hamdah, A.A. Amjad, E.M. Adel, A. Naushad, Facile one-pot green synthesis of Ag–ZnO nanocomposites using potato peel and their Ag concentration dependent photocatalytic properties, Sci. Rep. 10 (2020) 1–15, https://www.nature.com/articles/s41598-020-77426-y.

[58] R.O. Asriza, A. Indriawati, E. Julianti1, V.A. Fabiani, Synthesis and characterization of Fe_3O_4/SiO_2 nanocomposite from Kaolin Bangka Island, IOP Conf. Ser.: Earth Environ. Sci. 599 (2020) 1–6, http://dx.doi.org/10.1088/1755-1315/599/1/012063.

[59] S. Al-Ariki, N.A.A. Yahya, S.A. Al-A'nsi, M.H.H. Jumali, A.N. Jannah S.R. Shukor, Synthesis and comparative study on the structural and optical properties of ZnO doped with Ni and Ag nanopowders fabricated by sol gel technique, Sci. Rep. 11 (2021) http://dx.doi.org/10.1038/s41598-021-91439-1.

[60] I. Fatimah, F. Ganjar, S. Imam, K. Azlan, S. Suresh, D. Ruey-An, Nanoflflower-like composites of ZnO/SiO_2 synthesized using bamboo leaves ash as reusable photocatalyst, Arab. J. Chem. 14 (2021) 1–11, http://dx.doi.org/10.1016/j.arabjc.2020.102973.

[61] M. Appu, L. Zhifeng, Z. Dengqi, H. Jianying, Biosynthesis of chitosan-coated iron oxide (Fe_3O_4) hybrid nanocomposites from leaf extracts of Brassica oleracea L. and study on their antibacterial potentials, Biotech 11 (2021) 1–14, http://dx.doi.org/10.1007/s13205-021-02820-w.

[62] S.G. Mtavangu, R.R. Machunda, B. Bruggen, K.N. Njau, In situ facile green synthesis of Ag-ZnO nanocomposites using tetradenia riperia leaf extract and its antimicrobial efficacy on water disinfection, Sci. Rep. 12 (2022) 1–14, http://dx.doi.org/10.1038/s41598-022-19403-1.

[63] E. Prokhorov, L.B. Gabriel, M.Y.L. José, G.S. Alejandro, K. Yuriy, Chitosan-ZnO nanocomposites assessed by dielectric, mechanical, and piezoelectric properties, Polymers 12 (2020) 1–14, http://dx.doi.org/10.3390/polym12091991.